RSC Advances

PAPER

View Article Online
View Journal | View Issue

Cite this: *RSC Adv.*, 2024, **14**, 4116

Insights into the potential applications of permanganate/peroxymonosulfate systems: enhancement *via* amorphous MnO_2, effects of water matrices, and optimization using response surface methodology†

Xin Yang,[ac] Xiaoshuang Sun,[a] Jiang Yu,*[abc] Zhi Huang,[ac] Jie Yu,[ac] Siwei Deng,[a] Yinying Jiang[ab] and Weiwei Zhu[a]

Received 26th November 2023
Accepted 11th January 2024

DOI: 10.1039/d3ra08084f

rsc.li/rsc-advances

In this study, we developed a novel self-catalytic oxidation system involving peroxymonosulfate (PMS) and permanganate ($KMnO_4$), named as CUPP, to efficiently mineralize sulfamethoxazole (SMX) in groundwater. It was found that amorphous MnO_2 derived from the *in situ* reduction of $KMnO_4$ can directly adsorb HSO_5^-, a complex hydroxyl group, mediate the internal disproportionation reaction of HSO_5^- with the manganese complex, and effectively activate PMS, thereby promoting the oxidation of SMX and its degradation intermediates through sulfonate radiation. Furthermore, by using electron spin resonance (EPR), HPLC/MS full scan, and response surface methodology, the coexistence of $HO^{\bullet}$, $SO_4^{-\bullet}$, $O_2^{-\bullet}$, $^1O_2$, and active chlorine (Cl_2, HOCl) in the CUPP system was confirmed. A total of 24 intermediate products were detected, and four possible degradation pathways were identified for SMX. In addition, it was found that the CUPP system has a strong impact resistance to pH variations, groundwater anions, and natural organic matter stress. Undoubtedly, the CUPP system presents an innovative approach for the degradation of various emerging organic pollutants in groundwater.

1 Introduction

Sulfamethoxazole (SMX) is one of the earliest and most broadly used synthetic antibiotics and biocides, and is a typical sulfonamide antibiotic (SA).[1,2] In recent years, the detection of SMX in groundwater environments has become increasingly common worldwide, with concentrations ranging from ng L^{-1} to mg L^{-1}.[3,4] The persistence of residual SAs contributes to the proliferation and dissemination of antibiotic resistance genes and antibiotic-resistant bacteria, thereby posing significant biosafety risks.[2,5,6] Consequently, this matter has attracted widespread attention and concern. To address this issue, there is an immediate requirement for the development of reliable, safe, and efficient technologies capable of effectively degrading SMX in groundwater environments.

Peroxymonosulfate (PMS)-based *in situ* chemical oxidation (ISCO) is an emerging technology for soil and groundwater remediation that offers a wide range of applicability, rapid reaction rates, and mild reaction conditions.[7] It has demonstrated effectiveness in degrading antibiotics.[8] While PMS alone is not effective, it can be activated through methods such as alkali, heat, ultraviolet light, ultrasound, transition metals, carbon materials, and strong oxidants.[9–14] Activation generates sulfate radicals ($SO_4^{-\bullet}$),[15] which are highly capable of degrading a wide range of organic contaminants.[16] Manganese oxides, which are ubiquitously found as subsurface minerals, have garnered attention from scholars studying catalytic activation of PMS for organic contaminant degradation.[17] Saputra *et al.*[18] demonstrated the efficient activation of PMS using crystalline manganese oxides in various oxidation states, including Mn_3O_4, Mn_2O_3, MnO_2, and MnO, for the degradation of organic contaminants. Among these, MnO_2 is widely employed as a heterogeneous catalyst owing to its low toxicity, high catalytic efficiency, abundant sources, and diverse crystal structures.[19] However, the preparation of crystalline MnO_2 is a complex process, presenting a general challenge in terms of both preparation difficulty and large-scale application. Amorphous manganese dioxide MnO_2 (AMO) can be easily obtained through the self-reduction of permanganate (Mn(VII)) or the oxidation of dissolved manganese (Mn(II)).[20] Wang *et al.*[21]

[a]*Department of Environmental Science and Engineering, College of Architecture and Environment, Sichuan University, No. 24 South Section 1, Yihuan Road, Chengdu, 610065, P. R. China. E-mail: yuj@scu.edu.cn*

[b]*Yibin Institute of Industrial Technology, Sichuan University, Yibin 644000, P. R. China*

[c]*Institute of New Energy and Low Carbon Technology, Sichuan University, Chengdu, 610065, P. R. China*

† Electronic supplementary information (ESI) available. See DOI: https://doi.org/10.1039/d3ra08084f

conducted a study on the rapid degradation of bisphenol A using PMS in the presence of AMO. They proposed a non-radical mechanism involving the formation of reactive complexes between AMO and PMS. In the case of groundwater remediation, the delivery of solid catalysts to aquifers for PMS activation is time-consuming and impractical.[22] As such, the autocatalytic generation of reactive oxygen species (ROS) using *in situ* generated AMO through oxidative systems is undoubtedly a cost-effective and efficient catalytic pathway.

Permanganate ($KMnO_4$) is extensively employed for *in situ* chemical oxidation of organic contaminants in groundwater and soil due to its relative stability, wide adaptability across a broad pH range, generation of less hazardous by-products, and lower cost.[23,24] The permanganate oxidation technique, when employed alone, exhibits significant selectivity and proficiency in eliminating emerging contaminants that possess unsaturated bonds and electron-rich groups, but its efficacy in mineralizing other types of contaminants is somewhat restricted.[25–27] Studies have demonstrated that the combined use of $KMnO_4$ and PMS causes a synergistic effect on the mineralization of organic matter in solution, proving effective in degrading acid orange 7,[28] benzene, trichloroethylene,[22] and *p*-chlorobenzoic acid[29] in aqueous environments. This mechanism can be attributed to the activation of persulfate by permanganate and its reduction products, resulting in the production of ROS that facilitate efficient degradation of organic pollutants in the environment. Injecting aqueous $KMnO_4$ can increase the manganese content of groundwater or aquifers, potentially supporting *in situ* activation of PMS to enhance the ISCO effect on hard-to-degrade organic contaminants.[30] However, the mechanism of the $KMnO_4$/PMS system in micropollutant control in groundwater has not been systematically investigated, and there is a need to extend its effectiveness and applicability to the removal of a wide range of organic pollutants, which is essential for solving diverse environmental pollution problems.

In this study, we investigated the feasibility of the CUPP system, which combines $KMnO_4$ and PMS for the purpose of mineralizing organic contaminants in real groundwater. The study conducted laboratory batch experiments using the Box–Behnken experimental design, and employed advanced detection and analysis techniques, along with mathematical statistical methods, to assess the removal efficiency and oxidation characteristics of SMX when treated with the CUPP system. Additionally, our study unveiled the degradation mechanism of SMX in groundwater. The findings not only offer an innovative, cost-effective approach for *in situ* chemical oxidative remediation of antibiotics in groundwater, but also contribute to a deeper understanding of the CUPP system's applicability to a variety of organic pollutants.

2 Materials and methods

2.1 Chemicals and materials

SMX was purchased from PTSRTI, China. The chemical structure of SMX is shown in Fig. S1 of the ESI.† Oxone ($2KHSO_5 \cdot KHSO_4 \cdot K_2SO_4$) and other chemicals with purity ranging from 97% to 99.9% were purchased from CHENGDU SHUDU Chemical Reagent, China, and used as received. $KMnO_4$ was dissolved in deionized water to make a concentrated stock solution, which was boiled and stored in the dark. Prior to use, the $KMnO_4$ solution was determined by sodium oxalate titration. Other chemicals, purities, and suppliers are provided in Table S1.† All the stock solutions were prepared by dissolving the chemical agents into Milli-Q water prepared from a WP-UP-LH-10 Milli-Q system (Water Purifier, China).

2.2 Natural groundwater samples

Natural groundwater was sampled from a self-built water well built by a farmer in Shuangliu District, Chengdu City, Sichuan Province, China (103°54′50″, 30°38′36″). The natural groundwater was filtered by a 0.22 μm membrane filter and stored at 4 °C prior to use. The properties are provided in Table S2.†

2.3 Batch degradation experiments

The SMX oxidation experiments were conducted in a polypropylene centrifuge tube with screw cap. The chart of the batch oxidation experiment operating procedure is shown in Fig. S2.† A predetermined amount of SMX stock solution was mixed with the oxidants. The initial concentration of SMX was controlled at 5 mg L^{-1}, and the volume of the solution was kept at 50 mL. The temperature of the solution was maintained at 25 ± 1 °C by a water-bathing shaker, and continuous mechanical stirring was maintained throughout the reaction process with a stirring rate of about 180 rpm. If not otherwise specified, 10 mM phosphate buffer solution with a pH 7.0 was added into the reaction solution to control the pH before adding any oxidant. For the combined use of $KMnO_4$ and oxone, both were added into the reaction solution at the same time. Throughout the oxidation experiments, the solution was regularly sampled, and regularly sample the saturated $Na_2S_2O_3$ solution was added to quench the oxidation process. After that, excess $HONH_3Cl$ was added into the sample solution to convert the MnO_2 to Mn(II), avoiding the adsorption effect of amorphous MnO_2. The samples were filtered with a 0.22 μm filter membrane, and placed into a 1.5 mL serum bottle for testing. Acetate and borate buffer (10 mM) were used for pH 3.6–5 and pH 9, respectively. Three equal experiments were set, and the data referred to in this paper are the mean value.

2.4 Analytical methods

SMX was measured using a high-performance liquid chromatography instrument consisting of a Sapphiresil C18 HPLC pump (150 mm × 4.6 mm, 5 μm, FULI, China) and a UV/visible detector (detection wavelength 264 nm). The degradation intermediates and debris ions of SMX over a certain period of time were determined by high-performance liquid chromatography mass spectrometry (Waters 2695 HPLC, WatersZQ 2000 MS, USA). The pH value of the reaction solution was measured or monitored using a pH probe (PHS-25, INESA, China). The MnO_2 materials were characterized by scanning electron microscopy (SEM, Thermo Scientific Apreo 2 SEM, USA). For the SEM and EDS observation of amorphous MnO_2, a piece of nickel

foam was soaked in the solution for several seconds to collect the particles. Detailed information on the sample detection methods and AMO characterization methods are presented in Text S1.†

3 Results and discussion

3.1 Synergetic effect of the combined use of $KMnO_4$ and PMS

The degradation of SMX (5 mg L^{-1}) by PMS (6 mM) in the presence of $KMnO_4$ (6 mM) was investigated at pH 7. As depicted in Fig. 1, almost complete degradation of SMX was achieved within 30 min by the combination of $KMnO_4$ and PMS, while about 91.06% and 11.24% SMX were degraded by PMS alone and PM alone under identical conditions, respectively. These results suggested that $KMnO_4$ was an effective activator for PMS to degrade SMX. The degradation of SMX in the CUPP system was found to follow the single exponential model of the first-order kinetic law with the apparent rate constant (hereafter k_{obs}) of 0.23 min^{-1}. Comparatively, the k_{obs} for SMX degradation using PMS alone was 0.11 min^{-1}, with a considerably lower reaction rate and optimal degradation rate within 30 min. The results of the study confirmed that the CUPP system degraded SMX more completely and reacted more rapidly than the PMS or PM monooxygenation systems.

Based on these findings, it can be deduced that this phenomenon might be attributed to an increased presence of AMO secondary products generated by PM addition, subsequently activating PMS and promoting SMX degradation. However, as the PM concentration continues to rise, the secondary products compete with the SMX reaction sites, leading to no further improvement in the SMX degradation efficiency.[31,32]

3.2 Identification of the reactive oxidative species in the CUPP system

3.2.1 Radical quenching experiments. Due to activation, PMS, the primary component of oxone, can produce free radicals such as $HO^{\bullet}$ and $SO_4^{-\bullet}$ or non-free radicals such as $^1O_2$. Therefore, the active species in the reaction system were first determined by quenching tests, with methanol (MeOH) and *tert*-butanol (TBA) as trappers of $HO^{\bullet}$ and $SO_4^{-\bullet}$, trichloromethane ($CHCl_3$) as a trapper of $O_2^{-\bullet}$ (eqn (S1)–(S4)†),[33] L-tryptophan as a quencher of $^1O_2$, and NH_4^+ as a quencher of the active chlorine species.

As depicted in Fig. 2(a) and Table S3,† MeOH, TBA, and $CHCl_3$ all exert significant inhibitory effects on the degradation of SMX in the CUPP system. The quenching impact of MeOH and TBA on free radicals is essentially identical. With an increasing molar ratio of the two, the inhibition of SMX degradation becomes more pronounced. Conversely, the amount of $CHCl_3$ added did not affect the degradation of SMX. Thus, it can be inferred that $HO^{\bullet}$, $SO_4^{-\bullet}$, and $O_2^{-\bullet}$ coexist in the CUPP system, with $HO^{\bullet}$ and $SO_4^{-\bullet}$ assuming leading roles.

The presences of active chlorine compounds (Cl_2 and HOCl) and non-radical singlet oxygen ($^1O_2$) were also examined. The oxone compound, which serves as an oxidizing agent, incorporates 5% NaCl as an additional disinfection aid. Consequently, it is postulated that NaCl, acting as an auxiliary agent, might react with PMS to generate the active species, thereby facilitating the efficient degradation of SMX. For instance, in the Fe^{2+}/PMS system, the degradation of maleic acid is primarily driven by $SO_4^{-\bullet}$ in the absence of Cl^-. However, when the chloride ion concentration exceeds 5 mM, $Cl_2^{-\bullet}$ becomes the predominant free radical.[34] To confirm the presence of active chlorine, further verification experiments were conducted by adjusting the reaction solution and introducing different concentrations of NH_4^+ into the system. NH_4^+ reacts with HOCl to form chloramines (eqn (S5)–(S7)†). As illustrated in Fig. 2(d), the degradation efficiency of SMX decreased by 58%, 57%, and 56% upon increasing the NH_4^+ concentrations, compared to the control group. Given that NH_4^+ is a weaker oxidizing agent than HOCl, this suggests that the NH_4^+ addition significantly hinders SMX degradation, implicating the presence of HOCl as an active substance in this system. Fig. 2(b) demonstrates that the L-tryptophan addition considerably inhibits SMX degradation. Fig. 2(c) reveals that while 15 mM, 30 mM, and 60 mM L-tryptophan were added, the inhibitory effect increased positively compared to the control group, with the SMX degradation efficiency decreasing by 16%, 26%, and 49% within 45 min, respectively. This indicates that $^1O_2$ in the CUPP system may also be a dominant factor.

3.2.2 EPR analysis. In the CUPP system, active substances were identified using EPR with 5,5-dimethyl-1-pyrroline *N*-oxide (DMPO) and 2,2,6,6-tetramethylpiperidine (TEMP) as free radical scavengers. Fig. 3(a) reveals the distinct peaks of DMPO–OH and DMPO–SO_4^-, with four hydroxyl radical peaks exhibiting a 1 : 2 : 2 : 1 hyperfine splitting pattern.[35,36] Sulfate radical peaks of lower intensity were observed between the corresponding hydroxyl radical peaks, confirming the presence of $HO^{\bullet}$ and $SO_4^{-\bullet}$ in the reaction system. Fig. 3(b) displays six peaks (four prominent and two less intense) in a 1 : 1 : 1 pattern, characteristic of $O_2^{-\bullet}$.[37] In Fig. 3(c), the three distinct TEMP adduct peaks further indicate the presence of $^1O_2$ in the reaction solution.[37,38] Consequently, the CUPP system contains four active species: $HO^{\bullet}$, $SO_4^{-\bullet}$, $O_2^{-\bullet}$, and $^1O_2$. A substantial number of free radicals can be ascribed to the catalytic influence of *in situ* AMO on PMS and the self-decomposition of PMS. Although the quenching reaction does not entirely inhibit SMX

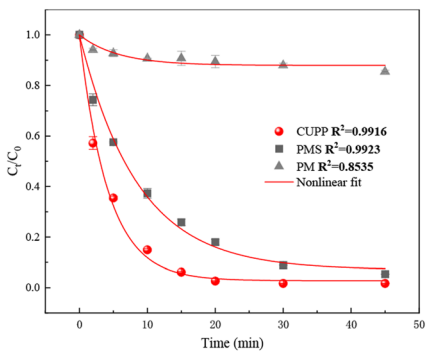

Fig. 1 Degradation of SMX in different treatment systems.

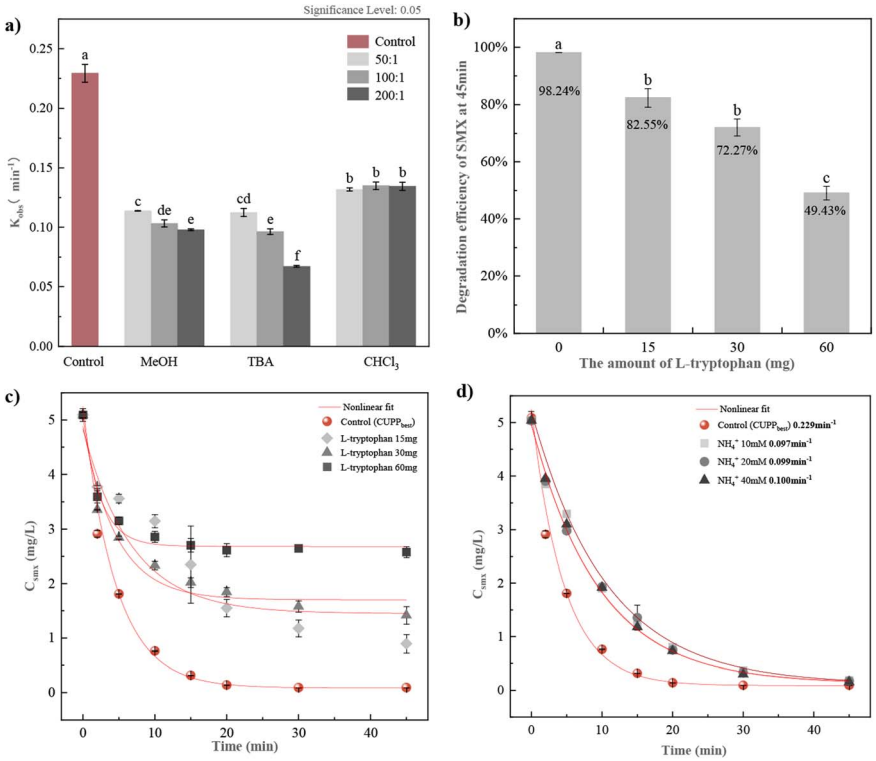

Fig. 2 (a) Indirect identification of radical active species. (b) Percentage degradation of SMX at 45 minutes of reaction time. (c) Effects of L-tryptophan on SMX degradation in the CUPP system. (d) SMX degradation rate after 45 min reaction. Note: labels at the top of the error bars indicate the level of statistical significance.

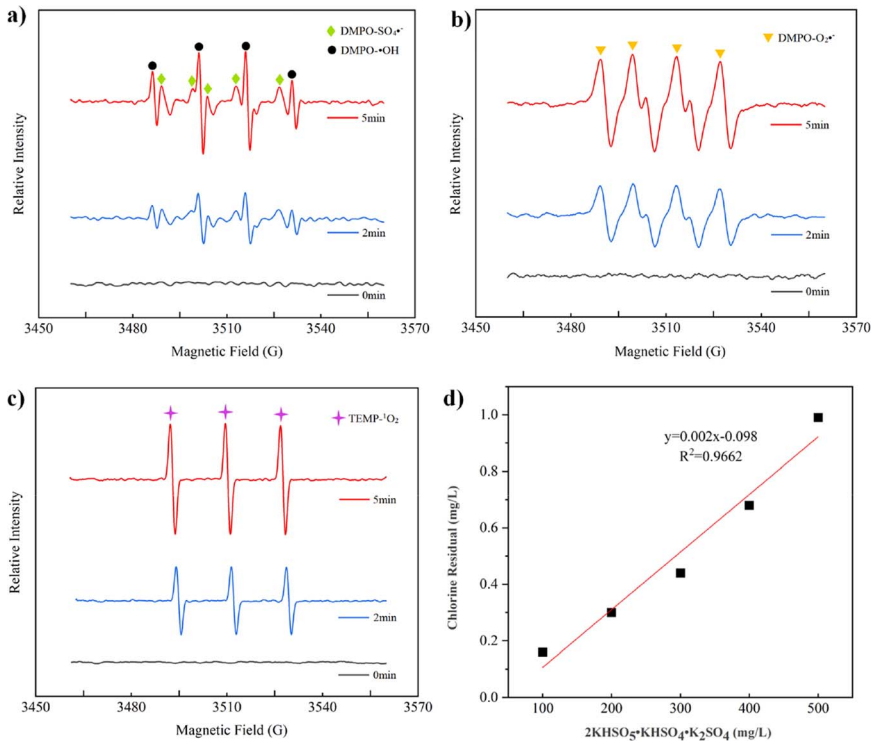

Fig. 3 (a) EPR detection mapping of $HO^{\bullet}$ and $SO_4^{-\bullet}$ (DMPO capture); (b) EPR profiling of $O_2^{-\bullet}$ (DMPO capture). (c) EPR assays of $^1O_2$ (TEMP capture). (d) Measurement of the residual chlorine concentration.

degradation in the CUPP system, $O_2^{-\bullet}$ can be converted into $^1O_2$, suggesting the presence of non-free radicals or other substances promoting the reaction.[39–41] Excess $HO^\bullet$ and $O_2^{-\bullet}$ in the system can generate $^1O_2$, and the intermediate products of the manganese peroxy complex will undergo internal disproportionation, producing $O_2^{-\bullet}$ and $^1O_2$.[42] Simultaneously, these products will react with the manganese complex to yield $SO_4^{-\bullet}$, accelerating the degradation rate of SMX. In examining the free radical generation mechanism of the MnO_2/PMS system, Xiao demonstrated that $^1O_2$ is produced not only from the subsequent transformation of $O_2^{-\bullet}$, but also directly through the MnO_2-induced activation of PMS.[43]

Oxone, as a complex, contains 5% chloride as a disinfectant in addition to PMS as the main source of the active substance. The primary influence of chloride ions (Cl^-) on the system is the formation of various halogen-based free radicals, which in turn decreases the system's oxidative capacity. An oxone solution with varying initial concentrations was prepared to directly investigate the efficacy of active chlorine as an active substance. As depicted in Fig. 3(d), a positive correlation exists between the active chlorine concentration and initial oxone concentration, indicating an increase in the residual chlorine concentration with increasing initial oxone concentration. This further corroborates that active chlorine is an essential oxidizing component in SMX degradation by the CUPP system. Zhang also suggested that the active chlorine species might be the active substance when investigating the impact of chloride ions on the oxone degradation of SMX in water.[33] While studying the effect of Cl^- on trichlorophenol degradation in the Co/PMS system, Xu *et al.*[44] found that Cl^- could generate Cl_2 and HOCl through oxidation *via* eqn (1) and (2). The promotion of SMX degradation in the CUPP system by chloride can be preliminarily attributed to the following three reasons: (i) chloride consumes $SO_4^{-\bullet}$, leading to the generation of a larger quantity of $HO^\bullet$. This results in a higher abundance of $HO^\bullet$ and relatively lower levels of $SO_4^{-\bullet}$ in the indirect identification outcomes; (ii) since $^1O_2$ serves as the primary active species, under alkaline conditions, oxone undergoes self-degradation or reacts with certain organic substances, generating $^1O_2$ that effectively oxidizes and degrades organic matter. Thus, even if Cl^- consumes a portion of $SO_4^{-\bullet}$, the reaction remains unaffected; (iii) under acidic conditions, Cl^- reacts with PMS to produce active chlorine, which promotes the oxidative degradation process of SMX.

$$2Cl^- + HSO_5^- + H^+ \rightarrow SO_4^{2-} + Cl_2 + H_2O \quad (1)$$

$$Cl^- + HSO_5^- \rightarrow SO_4^{2-} + HOCl \quad (2)$$

3.3 Mechanism analysis

3.3.1 Role of AMO. Through both free radical and non-free radical experiments, it was observed that no quenching agent could fully inhibit the reaction process of SMX degradation in the CUPP system. Consequently, it is concluded that $KMnO_4$, under the synergistic effect of PMS, may generate intermediate valence manganese, thereby enhancing the degradation efficiency of SMX. As depicted in Fig. 4(a), the black suspended matter formed during the experiment represents AMO. To further characterize the distribution of MnO_2 elements, EDS microregion analysis was performed, targeting points along the particle cross-section. The findings revealed atomic ratios of 32.26% for element O and 64.24% for element Mn, approximately equal to 2.0, suggesting a mixed oxide. During the experimental procedure, the black suspended particles produced as a result of the reaction were gathered using nickel foam, subsequently dried, and subjected to SEM scanning. As depicted in Fig. 4(a), the AMO affixed to the nickel foam surface exhibits a clustered arrangement comprising numerous sea urchin-like nanostructures.[28] With each individual nanostructure ranging in size from tens to hundreds of nanometers, this distinctive configuration imparts a larger specific surface area and facilitates excellent catalytic performance.

Based on these results, the synergistic effect between $KMnO_4$ and PMS in the CUPP system is as follows: the reaction of $KMnO_4$ generates amorphous manganese dioxide (eqn (3)), whose activation of PMS produces $SO_4^{-\bullet}$, which in turn oxidises SMX.[28] $SO_4^{-\bullet}$ can undergo a reaction with water or OH^- present in aqueous solutions or reaction systems, leading to the formation of hydroxyl radicals (eqn (4) and (5)). Furthermore, PMS exhibits distinctive redox properties and can be effectively activated by manganese oxides, such as crystalline manganese dioxide. The activation of PMS and the oxidation of organic compounds can be described by eqn (7) and (8), respectively.[29] Under the influence of $O_2^{-\bullet}$, $^1O_2$, $SO_4^{-\bullet}$, and $HO^\bullet$, SMX can undergo oxidation to yield various intermediate products, eventually resulting in the mineralization to CO_2 and H_2O (eqn (9)).

$$2MnO_4^- + 3HSO_5^- \rightarrow 2MnO_2 + 3O_2 + 3SO_4^{2-} + H^+ + H_2O \quad (3)$$

$$OH^- + SO_4^{-\bullet} \rightarrow SO_4^{2-} + HSO_5^- + HO^\bullet \quad (4)$$

$$H_2O + SO_4^{-\bullet} \rightarrow SO_4^{2-} + HO^\bullet + H^+ \quad (5)$$

$$2HSO_5^- + 2MnO_2 \rightarrow 2SO_5^{-\bullet} + Mn_2O_3 + H_2O \quad (6)$$

$$2HSO_5^- + Mn_2O_3 \rightarrow 2SO_4^{-\bullet} + 2MnO_2 + H_2O \quad (7)$$

$$O_2^-/^1O_2/HO^\bullet/SO_4^{-\bullet} + SMX \rightarrow CO_2 + H_2O \quad (8)$$

3.3.2 Transformation intermediates and pathways of SMX. The intermediates produced during the degradation of SMX by the CUPP system were analysed using HPLC/MS, in combination with the relevant data already reported in the literature. The HPLC/MS analysis identified 24 reaction intermediates and fragment ions, excluding the parent SMX ($m/z = 254$). The corresponding m/z values, molecular structure diagrams, and peak retention times for each compound are presented in Fig. S4.† Mass spectrogram evaluation reveals that the CUPP system employs a high concentration of ROS to target the SMX aromatic ring, initiating oxidation reactions. Electrophilic substitution, addition, elimination, and free radical coupling reactions contribute to the opening of benzene and pentane isoxazole

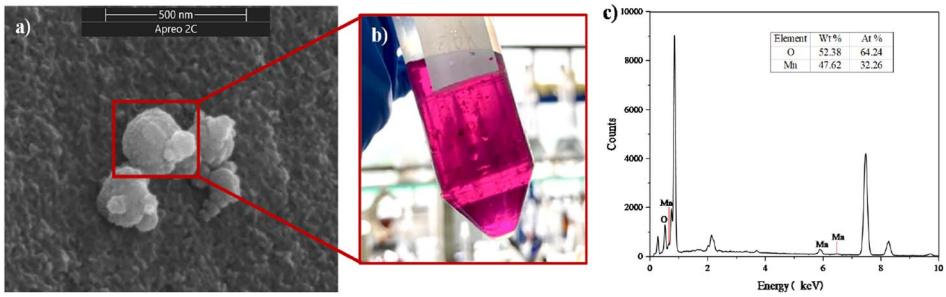

Fig. 4 (a) SEM electron microscopy of AMO. (b) Reaction solution production of AMO. (c) EDS spectrum.

rings, as well as the deprotonation of sulfonamide bonds. This process facilitates the further cleavage of S–N, N–O, S–N, and N–C bonds, generating various parent ions and multistage fragment ions. The degradation of SMX by CUPP generates intermediate products and fragment ions, which are outlined in Table S4.† Among these, five primary ions dominate, namely $C_{10}H_{11}O_5N_4S$ (**PA1**, $m/z = 299$), $C_9H_9O_6N_3S$ (**PB1**, $m/z = 301$), $C_{10}H_{11}O_4N_3S$ (**PC1**, $m/z = 284$), $C_{10}H_{11}O_3N_3S$ (**PD1**, $m/z = 270$), and $C_{10}H_{10}O_5N_3S$ (**PB2**, $m/z = 255$). The remaining 19 fragment ions result from the stepwise oxidative degradation of the parent ions. To elucidate the degradation mechanism of SMX in the primary CUPP system, we meticulously examined four potential degradation pathways (A, B, C, D), which are depicted in Fig. 5.

Degradation pathway A: **PA1** comprises two structures wherein the $-NO_2$ bond is positioned relative to the $-NH_3$ bond, either in the nearby or meso configurations. **PA2** corresponds to

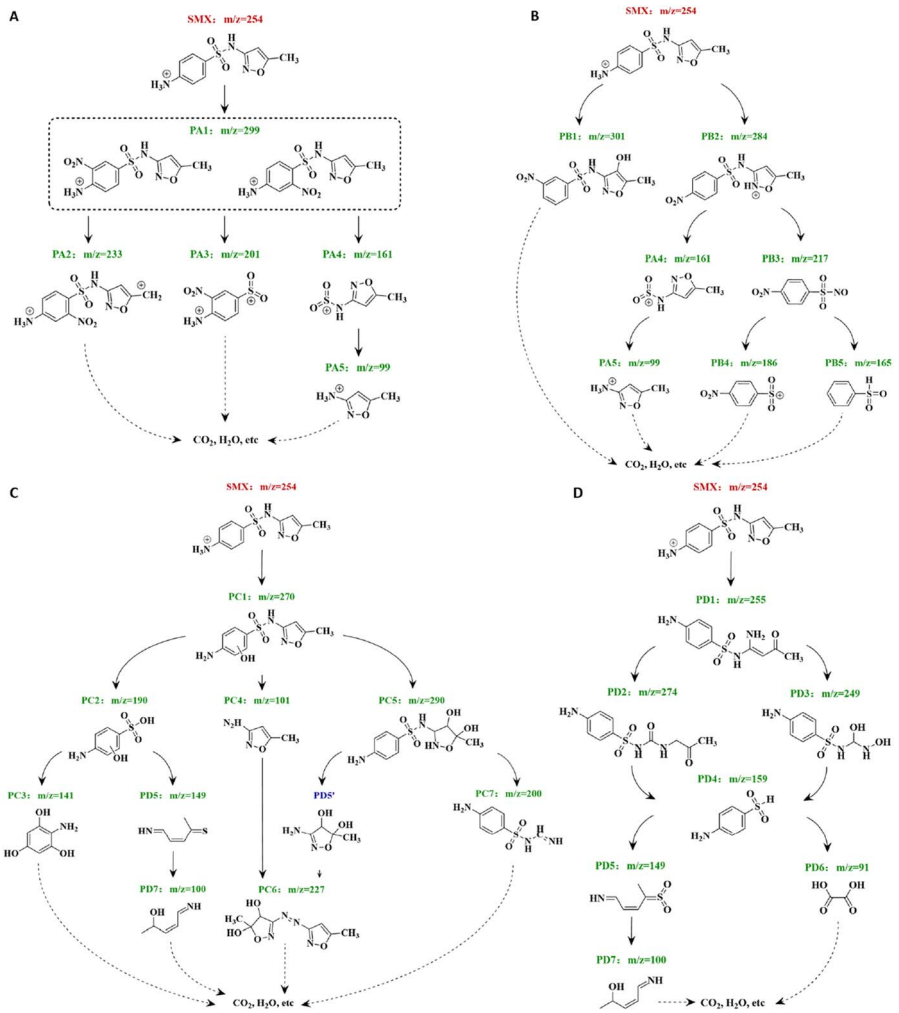

Fig. 5 Diagram of SMX degradation pathways (A–D).

the group formed subsequent to the elimination of H_2O_2S from **PA1**. **PA4** represents the group derived from **PA1**, following the breakage of the S–C bond and the loss of $C_6H_6O_2N_2$. Consequently, **PA4** undergoes attack by $SO_4^{-\bullet}$, resulting in the further loss of $C_6H_4O_4N_2S$, leading to the formation of **PA5** and SO_4^{2-}.

Degradation pathway B: this pathway is recognized as a common route for the degradation of SMX under the influence of $SO_4^{-\bullet}$. The primary $-NH_2$ on the benzene ring of SMX is directly oxidized to the $-NO_2$ by HOCl, $^1O_2$, and $SO_4^{-\bullet}$. Simultaneously, the five-membered ring is attacked by $HO^\bullet$, leading to the oxidation of the resulting products **PB1** and **PB2**. **PB1** has been identified as a significant product of SMX oxidation by $SO_4^{-\bullet}$, according to Yang *et al.*[45] The deprotonation of the sulfonamide bond in **PB2**, facilitated by the oxidation of $SO_4^{-\bullet}$ and $O_2^{-\bullet}$, leads to the cleavage of the N–C bond, resulting in the formation of **PA4** and **PB3**. Subsequently, **PB3** undergoes oxidation by $HO^\bullet$, continuing the elimination reaction and yielding **PB4**, **PB5**, and NO_3^-.

Degradation pathway C: although **PC5′** has not been detected in this study, it can be generated through the process of S–N bond breaking and is commonly detected during AOPs. This occurrence may be attributed to the high water solubility of **PC5′** and its strong reactivity with $SO_4^{-\bullet}$. Therefore, the structural formula of **PC5′** is temporarily utilized in this paper to fill the pathway.[46] This route is regarded as the classical degradation mechanism for SMX, involving $HO^\bullet$ and $SO_4^{-\bullet}$ attacking the C=C bond of the pentane isoxazole ring, undergoing electrophilic substitution and addition reactions to produce *ortho*-hydroxylated SMX (**PC1**). The aromatic ring carbon atoms in **PC1** are subsequently replaced by electrophilic $HO^\bullet$ to form **PC5**, while the S–N bond breakage generates **PC2** and **PC4**. The substitution reaction of **PC2** results in S–C bond cleavage, and hydrogen atoms in the aromatic ring are replaced by –OH, yielding **PC3**. Further oxidation of **PC2**'s aromatic ring leads to ring opening and formation of **PD6**, followed by the hydroxyl group replacing sulfur to produce **PD7**. **PC6** is hypothesized to form *via* the coupling of primary amino groups in **PC4** and **PC5′** compounds, centered on the N radical. Lastly, the oxazole ring of **PC5** is directly attacked by $SO_4^{-\bullet}$, creating **PC7**.

Degradation pathway D: this pathway involves the direct oxidation of $^1O_2$ with SO_4^- and the indirect oxidation of SMX by $HO^\bullet$. Initially, the oxazole ring of SMX is attacked and oxidized by $SO_4^{-\bullet}$, resulting in the breaking of the N–O bond. Subsequently, it is oxidized by $HO^\bullet$ to form **PD2** and **PD3**. These compounds then undergo sulfonamide bond deprotonation, leading to the breakage of the S–N bond and the formation of **PD4**. The benzene ring is further oxidized, resulting in the formation of the open ring compounds **PD5** and **PD6**. **PD5** undergoes an elimination and substitution reaction to produce **PD7** and SO_4^{2-}. According to Ghauch *et al.*,[47] the attack of $SO_4^{-\bullet}$ does not result in demethylation of the oxazole ring of SMX, unlike the attack of $HO^\bullet$. Instead, the oxazole ring is directly opened to form **PD1**.

3.4 Influencing factors on SMX oxidation

3.4.1 Effects of initial $KMnO_4$ and PMS concentrations and their ratio. The oxidant concentration is a crucial factor influencing the degradation rate of organic matter. As depicted in Fig. 6, the increase in oxone concentration initially leads to an increase in SMX degradation, followed by a subsequent decrease. Notably, when the oxone concentration reaches 6 mM, the degradation efficiency of SMX surpasses that of other concentration conditions (>90%). However, the decrease in SMX degradation rate resulting from excessive oxone concentration may be attributed to the self-quenching reaction of free radicals in the system, caused by excessive PMS concentration (eqn (9)–(11)).[48] This finding aligns with the research conclusion of Li.[49] Furthermore, although the degradation rate of SMX continues to rise with the increase in $KMnO_4$ concentration, the impact is limited in its effectiveness.

$$HSO_5^- + SO_4^{-\bullet} \rightarrow 2SO_5^{-\bullet} + SO_4^{2-} + H^+ \quad (9)$$

$$HSO_5^- + H_2O + SO_4^{-\bullet} \rightarrow 2SO_4^{2-} + HO_2^\bullet + 2H^+ \quad (10)$$

$$SO_4^{-\bullet} + SO_4^{-\bullet} \rightarrow S_2O_8^{2-} \quad (11)$$

Given the varying effects of utilizing the two oxidation systems individually in SMX degradation, this research endeavors to explore their combined impact and determine the optimal combination of the two systems. Based on the data presented in Fig. 7, the initial oxone concentration in the fixed CUPP system was 6 mM. It was observed that the degradation rate of SMX exhibited an upward trend as the $KMnO_4$ concentration increased within a 30 min. Notably, when the $KMnO_4$ concentration reached 2 mM, the degradation rate reached its peak at 98.9% and stabilized thereafter. Compared with PMS alone, the degradation efficiency of SMX in the CUPP system was significantly improved, and both were higher than that in the control group with PMS = 6 mM (91.06%), and the optimal concentration of PM in this case was 2 mM. It is evident that with a fixed $KMnO_4$ concentration of 2 mM, the degradation efficiency of SMX within 30 min exhibited an initial increase, followed by a decrease as the oxone concentration varied. Increasing the oxone concentration from 2 mM to 6 mM resulted in a 23% increase in the degradation efficiency,

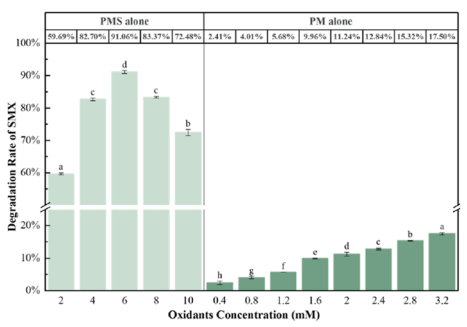

Fig. 6 Effects of oxone and $KMnO_4$ initial concentrations on SMX degradation (reaction conditions: $[SMX]_0$ = 5 mg L^{-1}, $[oxone]_0$ = 2–10 mM, $[KMnO_4]_0$ = 0.4–3.2 mM, pH_{ini} = 7.0 (10 mM phosphate buffer), and 25 °C; degradation rate was measured at 30 min). Note: labels at the top of the error bars indicate the level of statistical significance.

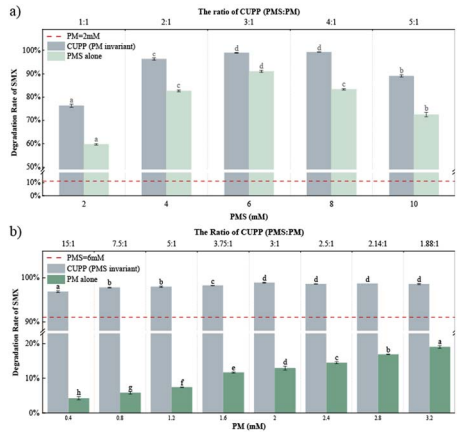

Fig. 7 (a) Effect of changing the oxone concentration on the SMX degradation in the PMS-alone system and CUPP system; (b) effect of changing the $KMnO_4$ concentration on the SMX degradation in the PM-alone system and CUPP system. Note: labels at the top of the error bars indicate the level of statistical significance.

reaching its maximum value. However, as the oxone concentration further increased from 6 mM to 10 mM, the SMX degradation rate gradually declined. By altering the oxone concentration, the molar ratio of oxidant in the CUPP system was varied as 1 : 1, 2 : 1, 3 : 1, 4 : 1, 5 : 1, respectively. Consequently, the degradation rate of SMX exhibited significant improvement compared to that of the PMS-alone system. Therefore, the CUPP system demonstrated superior effectiveness in treating SMX in groundwater, surpassing both the PM-alone and PMS-alone systems. The optimal ratio was found to be PMS : PM = 3 : 1 (PMS = 6 mM, PM = 2 mM).

3.4.2 Effect of pH. Solution pH affects the oxidation of the target compound by altering the speciation of both substrate and oxidant.[50,51] According to the data presented in Fig. 8, $KMnO_4$ displays a pronounced pH dependency, with the highest degradation rate (51%) observed at pH 3.6. Conversely, oxone and CUPP exhibit superior performance in alkaline conditions. Oxone achieves the highest degradation efficiency (94%) at pH 9, while CUPP attains an optimal degradation efficiency of 99%. Consequently, the CUPP system showcases a synergistic effect that remains unaffected by the pH of the reaction solution, thus demonstrating a remarkable ability to withstand fluctuations in acidity and alkalinity.

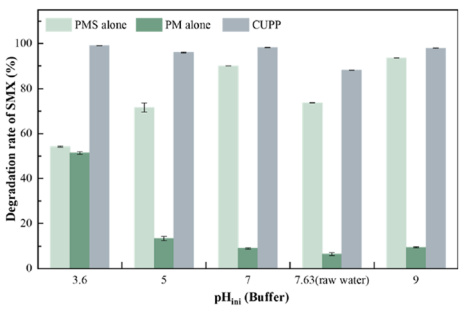

Fig. 8 Effects of pH on SMX degradation rate (reaction conditions: $[SMX]_0 = 5$ mg L^{-1}, $[oxone]_0 = 6$ mM, $[KMnO_4]_0 = 2$ mM, $pH_{ini} = 3.6$–9.0 (buffer), and 25 °C. Degradation rate was measured at 30 min).

Sulfamethoxazole exhibits two pK_a values corresponding to the protonation of aniline NH_2 ($pK_{a1} = 1.85$) and deprotonation of sulfonamide NH ($pK_{a2} = 5.60$), respectively.[52,53] The species distribution of SMX in water can be expressed as follows (eqn (12)):[54]

$$SMX + H^+ \overset{pK_{a1}}{\leftrightarrow} SMX \overset{pK_{a2}}{\leftrightarrow} SMX - H^- \quad (12)$$

where SMX + H^+, SMX, and SMX − H^- represent the cationic, neutral, and anionic species of SMX, respectively. In solution, the neutral form of SMX exists within the pH range of 1.85 < pH < 5.60. Below pH 1.85, the dominant form is the cationic SMX^+, while above pH 5.60, the dominant form is the anionic SMX^-. The enhanced transformation rate of SMX can be attributed to the deprotonation of the sulfonamide NH under moderate alkaline conditions, which activates the aniline moiety and facilitates electrophilic attack by oxidants such as PMS.[55] The concentration of each species is pH-dependent and can be described by the following equations:

$$\alpha^+ = \frac{[H^+]^2}{[H^+]^2 + K_{a1}[H^+] + K_{a1}K_{a2}} \quad (13)$$

$$\alpha^0 = \frac{K_{a1}[H^+]}{[H^+]^2 + K_{a1}[H^+] + K_{a1}K_{a2}} \quad (14)$$

$$\alpha^- = \frac{K_{a1}K_{a2}}{[H^+]^2 + K_{a1}[H^+] + K_{a1}K_{a2}} \quad (15)$$

where α^+, α^0, and α^- are the molar fractions of the cationic (SMX + H^+), neutral (SMX), and anionic (SMX − H^-) species, respectively. Therefore, the total concentration of SMX (*i.e.*, $[SMX]_{tot}$) can be calculated by eqn (16):

$$[SMX]_{tot} = \alpha^+[SMX]_0 + \alpha^0[SMX]_0 + \alpha^-[SMX]_0 \quad (16)$$

Therefore, preliminary deductions can be made regarding the potential degradation mechanisms of SMX in alkaline conditions. Notably, the addition of only PMS to the reaction solution leads to an enhanced degradation efficiency of SMX molecules as the pH transitions from acidic to alkaline. The results indicate that the buffer system yields superior outcomes, with pH 7 and 9 demonstrating the highest degradation efficiency. Given that the pH of the raw water is 7.63, the optimal condition is selected as the buffer system with a pH 7, which experiences minimal fluctuations.

3.4.3 Effects of NOM and inorganic anions. Groundwater comprises various anions and cations, which have the potential to exert an influence on the oxidative degradation of contaminants. In neutral or alkaline conditions, bicarbonate (HCO_3^-), chloride (Cl^-) and natural organic matter (NOM) are present as environmental background components.[56] The kinetic parameters of SMX degradation after adding Cl^-, HCO_3^- and humic acid (HA) into the CUPP system are shown in Table S5.†

Examining HA as a representative of NOM, the degradation of SMX by the CUPP system was explored at various dosages. As

depicted in Fig. 9(a) and (d), a slight decrease in the SMX removal rate occurred upon HA addition to the CUPP system, yet the removal rate increased with HA concentration. At an HA dosage of 50 mg L^{-1}, the degradation rate of SMX declined from 0.2219 min^{-1} to 0.17 min^{-1}. However, when the HA concentration reached 250 mg L^{-1}, the degradation rate increased to 0.19 min^{-1}. Based on the findings in Table S5,† it can be inferred that HA, functioning as a reductive macromolecular polymer, hinders or competes with the active substances or binding sites responsible for the degradation of SMX in the system. Therefore, it partially hinders the degradation process of SMX in the CUPP system, which is consistent with the results reported by Wu *et al.*[57] They observed a decrease in the efficiency of salicylic acid degradation caused by the reaction between HA and sodium hypochlorite in water. Nevertheless, this study discovered no significant correlation between the HA dosage and SMX degradation rate in the CUPP treatment process, with increased HA amounts reducing inhibitory effects. Consequently, the HA presence in groundwater would not severely impact the CUPP system's ability to degrade SMX.

Based on extensive literature reports, Cl^- in groundwater has been shown to partially impede pollutant degradation.[58] However, other studies have demonstrated that Cl^- can significantly enhance the degradation capacity of pollutants. For instance, Ji *et al.* discovered that low concentrations of Cl^- can efficiently degrade organic substances by generating active chlorine free radicals.[59] Conversely, high chloride concentrations may remove $SO_4^{-\bullet}$.[60] Fig. 9(b) and (e) illustrate the impact of the Cl^--free system on SMX degradation. Initially, this system yielded a k_{obs} of 0.2219 min^{-1}, resulting in a rapid degradation efficiency of 98% within 30 minutes. Subsequent introduction of Cl^- ions at concentrations of 5 mM, 7 mM, and 9 mM led to higher k_{obs} values of 0.26 min^{-1}, 0.36 min^{-1}, and 0.41 min^{-1}, respectively, surpassing those in the $CUPP_{best}$ control group. Remarkably, within just 15 minutes, the maximum degradation efficiency of 98.08%, 97.90%, and 97.57% were achieved, clearly indicating that Cl^- ions enhance the SMX degradation process within the CUPP system. Furthermore, this enhancing effect becomes more pronounced with increasing Cl^- concentrations, particularly when surpassing 3 mM. In light of Table S5,† it is evident that lower concentrations of added Cl^- have a negligible impact on the CUPP system. However, with an increase in the Cl^- concentration, k_{obs} exhibits a rapid ascent, highlighting the promoting effect of Cl^- on the degradation of SMX within the CUPP system. In previous studies involving the degradation of nitrophenol by the UV/PMS system,[61] as well as the removal of triclosan[62] and cephapirin[63] by the PDS/heat system, Cl^- was found to exhibit a dual effect of initial inhibition, followed by promotion. This phenomenon can be attributed to the formation of highly reactive chlorine species, such as chlorine free radicals ($Cl^\bullet$, $Cl_2^{-\bullet}$), and free active chlorine (Cl_2 and HOCl).[64] The concentration of non-radical active halogen species may be several orders of magnitude higher than that of $SO_4^{-\bullet}$. The specific reaction process is depicted in eqn (17)–(20). Moreover, $Cl^\bullet$ exhibits potent degradation capabilities towards electron-rich compounds,[65] and both HOCl and Cl_2 possess significant oxidative activity, enabling the rapid oxidation and degradation of organic pollutants. As the concentration of Cl^- increases, more Cl^- activates PMS, thereby enhancing the production of oxidizing agents and improving pollutant degradation efficiency. Upon introducing chloride to the CUPP system, the initial SMX degradation was hindered, potentially due to a low concentration threshold for Cl^- inhibition. In other words, at low Cl^- concentrations, Cl^- preferentially generates relatively weak $Cl^\bullet$. As the Cl^- concentration rises, the accumulated $Cl^\bullet$ reacts with Cl^- to form $Cl_2^{-\bullet}$. Furthermore, Cl^- can interact with PMS to produce active halogens Cl_2 or HOCl *via* double electron transfer, consequently expediting the SMX degradation process.

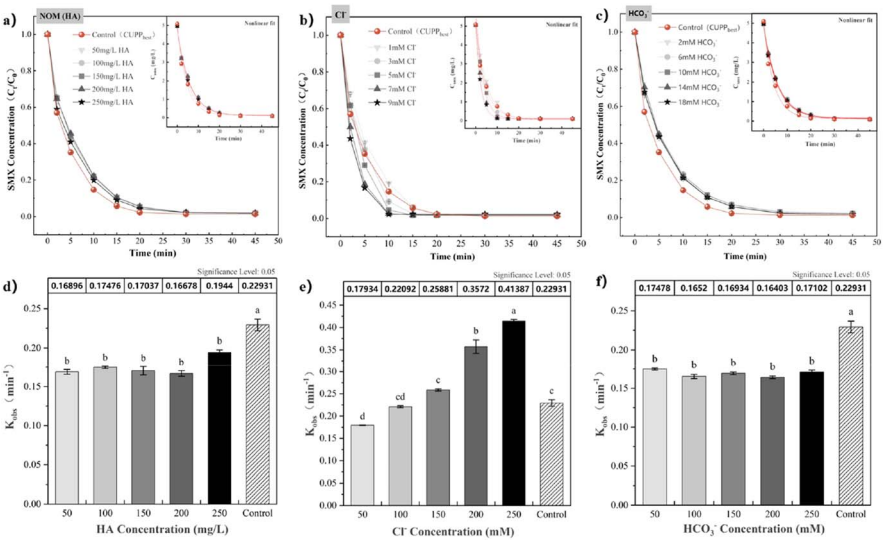

Fig. 9 (a–c) Degradation trend of SMX in the CUPP system under different HA, Cl^-, and HCO_3^- addition levels (embedded second-order kinetic fitting curve); (d–f) effects of HA, Cl^-, and HCO_3^- additions on the k_{obs} degradation of SMX by CUPP. Note: labels at the top of the error bars indicate the level of statistical significance.

$$SO_4^{-\bullet} + Cl^- \rightarrow SO_4^{2-} + Cl^\bullet \quad (17)$$

$$Cl^- + Cl^\bullet \rightarrow Cl_2^{-\bullet} \quad (18)$$

$$Cl^- + HO^\bullet \rightarrow ClOH^{-\bullet} \quad (19)$$

$$HOCl \rightarrow OCl^- + H^+ \quad (20)$$

The hydrolysis or dissociation of HCO_3^- occurs as the pH value of the water body changes, resulting in the production of H_2CO_3 or HCO_3^-.[49] HCO_3^- is commonly recognized as an active scavenging agent for $SO_4^{-\bullet}$ and $HO^\bullet$,[66] which adversely affects the degradation reactions of various activation types.[32,67,68] Consequently, this impact affects the solution's pH, the generation and capture of free radicals, ultimately leading to a decrease in the rate of free radical production and utilization. Based on Fig. 9(c) and (f), the presence of 2–18 mM HCO_3^- in the system leads to a decrease in the k_{obs} of SMX to 0.16–0.17 min^{-1}, and a delay in the time at which the maximum degradation rate of SMX occurs from 30 to 45 min. According to Table S4,† the addition of HCO_3^- significantly hinders the degradation reaction of the CUPP system towards SMX, although there is no significant correlation between the concentration and the reaction rate. The change in the pH value of the reaction solution influences the ionic state of organic pollutants in the solution, thereby promoting the degradation rate of organic pollutants. As illustrated in Fig. S3,† the addition of HCO_3^- initially raises the pH, and as the concentration increases from 2 mM to 18 mM, the pH value steadily climbs during the reaction. However, the pH consistently remains lower than the initial pH, while approaching it, indicating that HCO_3^- has minimal impact on the degradation process. It is hypothesized that the altered k_{obs} results from HCO_3^- elevating the OH^- concentration in the system, subsequently reducing the active chlorine generation and impeding the reaction. Concurrently, HCO_3^- can activate PMS, forming the two-electron compound HCO_4^-. Its relatively unstable oxygen–oxygen bond (–O–O–) readily dissociates into $CO_3^{-\bullet}$ and $HO^\bullet$. The oxidation of $HO^\bullet$ typically compensates for the system's active chlorine deficiency, preventing further inhibition as the HCO_3^- concentration increases. Potential reactions within the system are represented in eqn (23) and (24). Based on the aforementioned results, it is evident that the CUPP system demonstrates superior resilience to changes in the groundwater environment, and possesses heightened environmental adaptability.

$$CO_3^{2-} + H_2O \rightarrow HCO_3^- + OH^- \quad (21)$$

$$HCO_3^- + H_2O \rightarrow H_2CO_3 + OH^- \quad (22)$$

$$HCO_3^- + HSO_5^- \rightarrow SO_4^{2-} + H^+ + HCO_4^- \quad (23)$$

$$HCO_4^- \rightarrow CO_3^{-\bullet} + HO^\bullet \quad (24)$$

3.5 Optimization of the CUPP system based on RSM

This study employed the response surface methodology (RSM) method based on the Box–Behnken design (BBD) to analyze and model the main influencing factors in the degradation of SMX in groundwater. The experimental design scheme and response surface results are presented in Table S6.† The final quadratic regression equation results of the degradation fitting model are shown in the following eqn (25) ($R^2 = 0.9892$):

$$Y_{k_{obs}} = 0.23 + 0.022A + 0.013C + 0.013AB - 0.012AC - 0.037A^2 - 0.035B^2 \quad (25)$$

where A represents PMS, B represents PM, and C represents pH, and the multiplication of the two coefficients represents the interaction. The results of the quadratic model variance

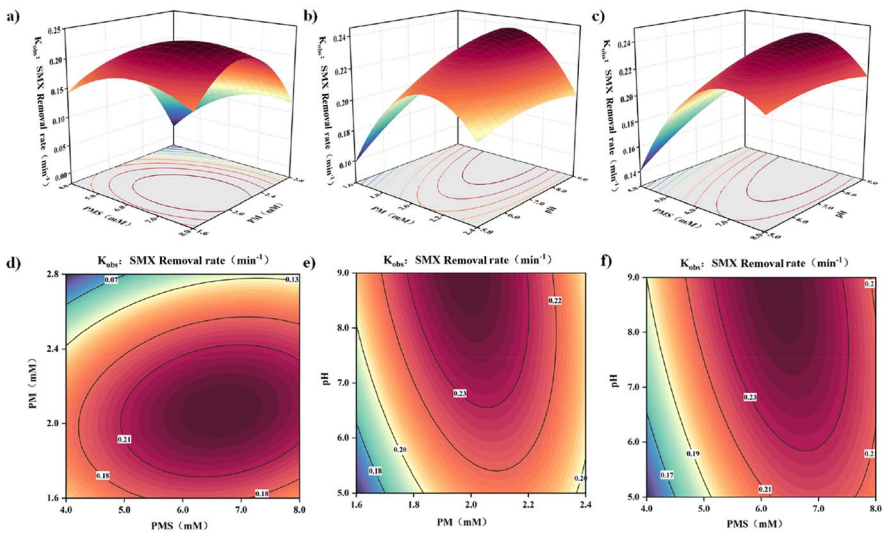

Fig. 10 The interaction response surface between the PMS concentration, PM concentration, and pH: (a–c) contour line; (d–f) 3D surface diagram.

analysis (Tables S7 and S8†) indicate high significance, with a confidence level greater than 95% and a *P*-value less than 0.0001. The probability of noise-induced deviation is only 0.01%, demonstrating a strong level of fitting. The *P*-value for the missing factor is greater than 0.05, indicating no significant missing factor. The adeq. precision is 23.647, confirming that the adopted signal proportion meets the requirements within the determined space range. Therefore, the predicted values from this model are reliable. Additionally, the residual four-in-one graph of the model (Fig. S5†) demonstrates a significant linear correlation among the data points, with a high R^2 value of 0.9892 achieved through fitting with $y = x$. The findings demonstrate the RSM model's capability to accurately describe and predict the efficiency and influencing factors of SMX oxidation removal from groundwater using the CUPP system. The model was employed to forecast the impact of three key factors (pH, PMS, PM) on the degradation of SMX in groundwater through CUPP oxidation removal. Based on the Pareto chart's main effect analysis (Fig. S6†), the interaction between the two influencing factors was ranked as follows: PMS > pH > PM.

Furthermore, based on the fitted binary regression equation, a response surface curve and corresponding contour plot were constructed (Fig. 10). The steepness of the surface slope in the response surface 3D map indicates the strength of the interaction between the two factors, while the shape of the contours directly reflects the magnitude of the interaction. For instance, greater curvature of the elliptic contours signifies a stronger interaction between the factors. The graphical results reveal significant correlations in the interaction effects of PMS (*A*), PM (*B*), and pH (*C*). Moreover, the observed trends and degradation effects of SMX align closely with the outcomes of the single-factor experiments, thereby further validating the accuracy of the experimental findings.

In general, the model predicted the optimal degradation conditions as [oxone] = 6.3 mM, [$KMnO_4$] = 1.99 mM, and pH = 8.92. Under these conditions, the predicted optimal response value was 0.24 min^{-1}, with a minimal difference of only 1.425% between k_{obs} and the predictor. This demonstrates the RSM model's strong predictive accuracy. These optimal conditions offer valuable insights for practical applications.

4 Conclusions

The focus of this research pertained to the utilization of an innovative self-catalytic oxidation system, combining peroxymonosulfate and permanganate, for the examination of the degradation of the emerging groundwater contaminant, sulfamethoxazole. The main findings are as follows: (i) laboratory-scale batch experiments unveiled the exceptional performance of the CUPP system. Under optimized reaction conditions ([PMS] = 6 mM, [PM] = 2 mM, pH_{ini} = 7.0, $[SMX]_0$ = 5 mg L^{-1}, T = 25 °C), SMX exhibited a degradation efficiency of 98.9%, a substantial improvement compared to the lower degradation rates achieved when employing PMS or PM individually. (ii) The CUPP system followed a second-order single exponential kinetics model (R^2 = 0.9916), indicating its remarkable degradation efficiency and capacity for pH regulation. (iii) The formation of a distinctive black agglomerative secondary product, identified as AMO, was observed. This secondary product possesses a unique sea urchin nanostructure, which enhances its specific surface area, thereby contributing to elevated catalytic performance. This observation substantiates the *in situ* activation and degradation of organic pollutants by natural manganese ore. (iv) The investigation utilized chemical probes and EPR to identify ROS. HPLC/MS detected degradation intermediates and fragments, revealing four SMX degradation pathways and their underlying mechanisms. (v) The impact of key anions and NOM in groundwater on the SMX degradation was also investigated, and the results revealed the adaptability of the CUPP system to environmental variations. (vi) The response surface methodology was applied to validate the accuracy of the model, analyze regression coefficients, and optimize the process conditions. Subsequent verification confirmed the optimal operational parameters as follows: [PMS] = 6.30 mM, [PM] = 1.99 mM, and pH_{ini} = 8.92. In conclusion, this research underscores the efficacy of the CUPP system in the degradation of SMX, offering a promising approach for addressing emerging groundwater pollutants. The study's comprehensive investigation into reaction kinetics, reaction intermediates, and environmental adaptability provides valuable insights into the practical application of this novel oxidation system.

Author contributions

All authors contributed to the study conception and design. The experiment was carried out by Xin Yang, Xiaoshuang Sun, Zhi Huang, Jie Yu, and Yinying Jiang. Material preparation, data collection and analysis were performed by Xin Yang, Xiaoshuang Sun, Jiang Yu, Siwei Deng, and Weiwei Zhu. The first draft of the manuscript was written by Xin Yang and Xiaoshuang Sun. All authors commented on previous versions of the manuscript. All authors read and approved the final manuscript.

Conflicts of interest

There are no conflicts to declare.

Acknowledgements

The research was supported by the National Key Research and Development Program (No. 2018YFC1802605), the Sichuan Regional Innovation Cooperation Project (No. 2022YFQ0081), the Chengdu Key R&D Support Plan Project (No. 2022-YF05-00357-SN), and the Sichuan University-Yibin City School and City Strategic Cooperation Project (No. 2020CDYB-9).

Notes and references

1 D. T. Oyekunle, E. A. Gendy, J. Ifthikar and Z. Chen, *Chem. Eng. J.*, 2022, **437**, 135277.
2 Amina, Q. Abbas, A. Shakoor, M. Naushad and B. Yousaf, *Process Saf. Environ. Prot.*, 2022, **164**, 696–705.

3 H. Wang, W. Guo, R. Yin, J. Du, Q. Wu, H. Luo, B. Liu, F. Sseguya and N. Ren, *Chem. Eng. J.*, 2019, **362**, 561–569.
4 F. Huang, Z. An, M. J. Moran and F. Liu, *J. Hazard. Mater.*, 2020, **399**, 122813.
5 Z. Liu, L. Ge, K. Wang, H. Yin, D. Li, S. Yang, G. Wang and D. Miao, *J. Water Proc. Eng.*, 2023, **53**, 103781.
6 J. Yan, J. Peng, L. Lai, F. Ji, Y. Zhang, B. Lai, Q. Chen, G. Yao, X. Chen and L. Song, *Environ. Sci. Technol.*, 2018, **52**, 14302–14310.
7 Y. Ji, C. Ferronato, A. Salvador, X. Yang and J.-M. Chovelon, *Sci. Total Environ.*, 2014, **472**, 800–808.
8 D. T. Oyekunle, E. A. Gendy, J. Ifthikar and Z. Chen, *Chem. Eng. J.*, 2022, **437**, 135277.
9 J. Sharma, I. M. Mishra, D. D. Dionysiou and V. Kumar, *Chem. Eng. J.*, 2015, **276**, 193–204.
10 W.-D. Oh, Z. Dong and T.-T. Lim, *Appl. Catal., B*, 2016, **194**, 169–201.
11 F. Ghanbari and M. Moradi, *Chem. Eng. J.*, 2017, **310**, 41–62.
12 F. Soumia and C. Petrier, *Ultrason. Sonochem.*, 2016, **32**, 343–347.
13 C. Qi, X. Liu, J. Ma, C. Lin, X. Li and H. Zhang, *Chemosphere*, 2016, **151**, 280–288.
14 Y. Yang, J. Jiang, X. Lu, J. Ma and Y. Liu, *Environ. Sci. Technol.*, 2015, **49**, 7330–7339.
15 L. Chen, X. Hu, Y. Yang, C. Jiang, C. Bian, C. Liu, M. Zhang and T. Cai, *Chem. Eng. J.*, 2018, **351**, 523–531.
16 Y. Zhou, Y. Xiang, Y. He, Y. Yang, J. Zhang, L. Luo, H. Peng, C. Dai, F. Zhu and L. Tang, *J. Hazard. Mater.*, 2018, **359**, 396–407.
17 J. X. Li, Q. X. Shi, R. Zhao, Y. Liu, J. J. Chen, J. M. Liu, P. P. Liu and J. P. Jia, *Environ. Chem.*, 2023, 1–17.
18 E. Saputra, S. Muhammad, H. Sun, H.-M. Ang, M. O. Tadé and S. Wang, *Appl. Catal., B*, 2013, **142–143**, 729–735.
19 E. Saputra, S. Muhammad, H. Sun, A. Patel, P. Shukla, Z. H. Zhu and S. Wang, *Catal. Commun.*, 2012, **26**, 144–148.
20 X. Huangfu, J. Jiang, J. Ma, Y. Liu and J. Yang, *Environ. Sci. Technol.*, 2013, **47**, 10285–10292.
21 L. Wang, J. Jiang, S.-Y. Pang, Y. Zhou, J. Li, S. Sun, Y. Gao and C. Jiang, *Chem. Eng. J.*, 2018, **352**, 1004–1013.
22 J. Cui, L. Zhang, B. Xi, J. Zhang and X. Mao, *Chem. Eng. J.*, 2017, **313**, 815–825.
23 R. H. Waldemer and P. G. Tratnyek, *Environ. Sci. Technol.*, 2006, **40**, 1055–1061.
24 S. H. Liang, K. F. Chen, C. S. Wu, Y. H. Lin and C. M. Kao, *Water Res.*, 2014, **54**, 149–158.
25 J. Zhang, B. Sun and X. Guan, *Sep. Purif. Technol.*, 2013, **107**, 48–53.
26 L. Hu, A. M. Stemig, K. H. Wammer and T. J. Strathmann, *Environ. Sci. Technol.*, 2011, **45**, 3635–3642.
27 J. Jiang, S.-Y. Pang, J. Ma and H. Liu, *Environ. Sci. Technol.*, 2012, **46**, 1774–1781.
28 S. Gao, J. Cui, Y. Xiong, W. Xiao, D. Wang, A. N. Alshawabkeh and X. Mao, *Sep. Purif. Technol.*, 2015, **144**, 248–255.
29 L. Wang, J. Jiang, S.-Y. Pang, Y. Gao, Y. Zhou, J. Li, Y. Yang, J. Ma and T. Zhang, *Chemosphere*, 2019, **228**, 602–610.
30 L. Bridges, R. A. M. Mohamed, N. A. Khan, M. L. Brusseau and K. C. Carroll, *Water*, 2020, **12**, 3061.
31 E. Saputra, S. Muhammad, H. Sun, H. M. Ang, M. O. Tadé and S. Wang, *Environ. Sci. Technol.*, 2013, **47**, 5882–5887.
32 E.-T. Yun, H.-Y. Yoo, H. Bae, H.-I. Kim and J. Lee, *Environ. Sci. Technol.*, 2017, **51**, 10090–10099.
33 M. W. Zhang, Master, Xinjiang University, 2020.
34 T. Q. Li, Master, Qingdao University, 2022.
35 W.-Q. Li, Y.-X. Wang, J.-Q. Chen, N.-N. Hou, Y.-M. Li, X.-C. Liu, R.-R. Ding, G.-N. Zhou, Q. Li, X.-G. Zhou and Y. Mu, *Appl. Catal., B*, 2022, **302**, 120882.
36 D. Wang, M. Suo, S. Lai, L. Deng, J. Liu, J. Yang, S. Chen, M.-F. Wu and J.-P. Zou, *Appl. Catal., B*, 2023, **321**, 122054.
37 M. Li, S. You, X. Duan and Y. Liu, *Appl. Catal., B*, 2022, **312**, 121419.
38 Y. Chen, X. Bai, Y. Ji and D. Chen, *J. Hazard. Mater.*, 2023, **441**, 129912.
39 C. Chen, L. Liu, Y. Li, W. Li, L. Zhou, Y. Lan and Y. Li, *Chem. Eng. J.*, 2020, **384**, 123257.
40 X. Cheng, H. Guo, Y. Zhang, X. Wu and Y. Liu, *Water Res.*, 2017, **113**, 80–88.
41 M. P. Rayaroth, K. P. Prasanthkumar, Y.-G. Kang, C.-S. Lee and Y.-S. Chang, *Chem. Eng. J.*, 2020, **382**, 122828.
42 S. Zhu, X. Li, J. Kang, X. Duan and S. Wang, *Environ. Sci. Technol.*, 2019, **53**, 307–315.
43 G. F. Xiao, PhD, China University of Geosciences, 2021.
44 L. Xu, R. X. Yuan, Y. G. Guo, D. X. Xiao, Z. H. Wang and J. S. Liu, *J. Wuhan Univ., Nat. Sci. Ed.*, 2013, **59**, 51–56.
45 Y. Yang, X. Lu, J. Jiang, J. Ma, G. Liu, Y. Cao, W. Liu, J. Li, S. Pang, X. Kong and C. Luo, *Water Res.*, 2017, **118**, 196–207.
46 J. S. Du, PhD, Harbin Institute of Technology, 2019.
47 A. Ghauch, G. Ayoub and S. Naim, *Chem. Eng. J.*, 2013, **228**, 1168–1181.
48 X. Chen, J. Zhou, H. Yang, H. Wang, H. Li, S. Wu and W. Yang, *Chemosphere*, 2022, **287**, 132074.
49 W. Z. Li, Master, Jiangnan University, 2022.
50 V. K. Sharma, S. K. Mishra and N. Nesnas, *Environ. Sci. Technol.*, 2006, **40**, 7222–7227.
51 L. Hu, H. M. Martin and T. J. Strathmann, *Environ. Sci. Technol.*, 2010, **44**, 6416–6422.
52 A. L. Boreen, W. A. Arnold and K. McNeill, *Environ. Sci. Technol.*, 2004, **38**, 3933–3940.
53 Z. Qiang and C. Adams, *Water Res.*, 2004, **38**, 2874–2890.
54 Y. Ji, J. Lu, L. Wang, M. Jiang, Y. Yang, P. Yang, L. Zhou, C. Ferronato and J.-M. Chovelon, *Water Res.*, 2018, **147**, 82–90.
55 M. C. Dodd, M.-O. Buffle and U. von Gunten, *Environ. Sci. Technol.*, 2006, **40**, 1969–1977.
56 A. Li, Z. Wu, T. Wang, S. Hou, B. Huang, X. Kong, X. Li, Y. Guan, R. Qiu and J. Fang, *J. Hazard. Mater.*, 2018, **357**, 207–216.
57 Z. Wu, X. Zhang, J. L. Pang, H. Y. Liu and P. Y. Zhang, *Ind. Water Wastewater*, 2019, **50**, 5–8.
58 Y. H. Guan, W. J. Sun and P. P. Wang, *J. Harbin Inst. Technol.*, 2022, **54**, 50–58.
59 Y. Ji, C. Dong, D. Kong, J. Lu and Q. Zhou, *Chem. Eng. J.*, 2015, **263**, 45–54.
60 X.-Y. Yu, Z.-C. Bao and J. R. Barker, *J. Phys. Chem. A*, 2004, **108**, 295–308.

61 J. Zhou, J. H. Xiao, C. L. Fang, D. X. Xiao, Y. G. Guo, X. Y. Lou, Z. H. Wang and J. S. Liu, *Chin. J. Environ. Sci.*, 2016, **36**, 66–73.
62 H. Gao, J. Chen, Y. Zhang and X. Zhou, *Chem. Eng. J.*, 2016, **306**, 522–530.
63 Y. Qian, G. Xue, J. Chen, J. Luo, X. Zhou, P. Gao and Q. Wang, *J. Hazard. Mater.*, 2018, **354**, 153–160.
64 M. Wu, Z. Xu, W. Wu, D. Tian, J. B. Chen and T. Y. Huang, *Technol. Water Treat.*, 2019, **45**, 64–68.
65 Y. Xue, Z. Wang, R. Naidu, R. Bush, F. Yang, J. Liu and M. Huang, *Chem. Eng. J.*, 2022, **433**, 134546.
66 Y. M. Li, Master, Sichuan Agricultural University, 2018.
67 F. Vicente, A. Santos, A. Romero and S. Rodriguez, *Chem. Eng. J.*, 2011, **170**, 127–135.
68 K.-C. Huang, R. A. Couttenye and G. E. Hoag, *Chemosphere*, 2002, **49**, 413–420.